Mechanical strength of boron nitride nanotube-polymer interfaces

Xiaoming Chen,[1] Liuyang Zhang,[2] Cheol Park,[3,4] Catharine C. Fay,[3] Xianqiao Wang,[2,a)] and Changhong Ke[1,a)]
[1]*Department of Mechanical Engineering, State University of New York at Binghamton, Binghamton, New York 13902, USA*
[2]*College of Engineering, University of Georgia, Athens, Georgia 30602, USA*
[3]*NASA Langley Research Center, Hampton, Virginia 23681, USA*
[4]*Department of Mechanical and Aerospace Engineering, University of Virginia, Charlottesville, Virginia 22904, USA*

(Received 27 September 2015; accepted 13 November 2015; published online 22 December 2015)

We investigate the mechanical strength of boron nitride nanotube (BNNT) polymer interfaces by using *in situ* electron microscopy nanomechanical single-tube pull-out techniques. The nanomechanical measurements show that the shear strengths of BNNT-epoxy and BNNT-poly(methyl methacrylate) interfaces reach 323 and 219 MPa, respectively. Molecular dynamics simulations reveal that the superior load transfer capacity of BNNT-polymer interfaces is ascribed to both the strong van der Waals interactions and Coulomb interactions on BNNT-polymer interfaces. The findings of the extraordinary mechanical strength of BNNT-polymer interfaces suggest that BNNTs are excellent reinforcing nanofiller materials for light-weight and high-strength polymer nanocomposites. © *2015 AIP Publishing LLC*. [http://dx.doi.org/10.1063/1.4936755]

The quest for light, strong, and durable composite materials is of importance for a number of industries, such as the aerospace and automobile industries. The interfacial load transfer capacity of nanofiller-polymer interfaces plays a critical role in the bulk performance of fiber-reinforced polymer nanocomposites, and thus a primary factor in the selection of reinforcing nanofiller materials. This is because adequate load transfer from polymer to fibers demands a strong fiber-polymer interface.[1,2] Boron nitride nanotubes (BNNTs)[3,4] are a type of light, strong, thermally and chemically stable tubular nanostructure, and have received increasing attention among all types of reinforcing nanofillers that are investigated for polymer nanocomposites.[5] Research has shown that BNNTs possess a Young's modulus of up to 1.3 TPa and a tensile strength of up to 33 GPa,[6–15] both of which are comparable with their pure carbon counterpart, carbon nanotubes (CNTs). Conceptually, it is envisioned that BNNTs are capable of forming strong binding interfaces with polymers, which is partially due to their highly polarized electrical characteristics,[16] and the resulting strong Coulomb interactions with polymers. However, the mechanical strength of BNNT-polymer interfaces remains largely unexplored to date. Here, we investigate the mechanical strength of BNNT-polymer interfaces by using *in situ* electron microscopy nanomechanical single-tube pull-out techniques. The nanomechanical measurements reveal superior interfacial load transfer capacity on BNNT-epoxy and BNNT-poly(methyl methacrylate) (PMMA) interfaces. Molecular dynamics (MD) simulations are performed to provide insights into the BNNT-polymer interfacial binding mechanism.

Figure 1(a) illustrates the *in situ* electron microscopy nanomechanical single-tube pull-out scheme, which was demonstrated in our recent studies of CNT-polymer interfaces.[17,18] In this testing scheme, the BNNT-polymer interface is engineered inside a sandwiched polymer-tube-polymer thin-film composite. A protruding tube is stretched by an incrementally displaced atomic force microscopy (AFM) cantilever until the embedded tube segment is pulled out of the polymer matrix. To ensure a pure-stretching pull-out, only those protruding tubes that are oriented parallel to the stretching force direction are selected for pull-out measurements. The nanomechanical pull-out tests were performed inside an FEI Nanolab 600 scanning electron microscope (SEM). Silicon AFM probes (model CSG 01, NT-MDT) were employed as the force sensors, and their spring constants were calibrated individually and are within the range of 0.04–0.09 N/m. The AFM sensor was mounted to a 3D piezo stage that possesses 1 nm displacement resolution in the X-Y-Z axes.

The BNNTs employed in this study were synthesized using High-temperature Pressure (HTP) methods,[19,20] and were separated/dispersed in deionized (DI) water by ultrasonication with the aid of ionic surfactants.[21,22] AFM studies show that a majority of the dispersed BNNTs are less than 2 μm in length and maintain reasonable straightness when deposited on flat substrates. The diameters of the dispersed tubes are found to be polydispersed, as shown by the histogram in Figure 1(b). The median tube diameter is 2.9 nm, and >80% of the tubes have diameters within the range of 1.9–3.9 nm, which are well-correlated with the diameter of double-walled BNNTs.[22] Surface chemistry of the dispersed BNNTs were examined using Fourier transform infrared (FTIR) and Raman spectroscopy, and no noticeable chemical groups on BNNT surfaces were detected (see Figure S1 in supplementary material[43]). Epon 828 epoxy resin with curing agent EPIKURE 3200 aminoethyl piperazine (AEP) (Momentive Specialty Chemicals Inc.) and PMMA (50 000 in molecular weight, Sigma-Aldrich) are the two types of

a)Authors to whom correspondence should be addressed. Electronic addresses: xqwang@uga.edu and cke@binghamton.edu

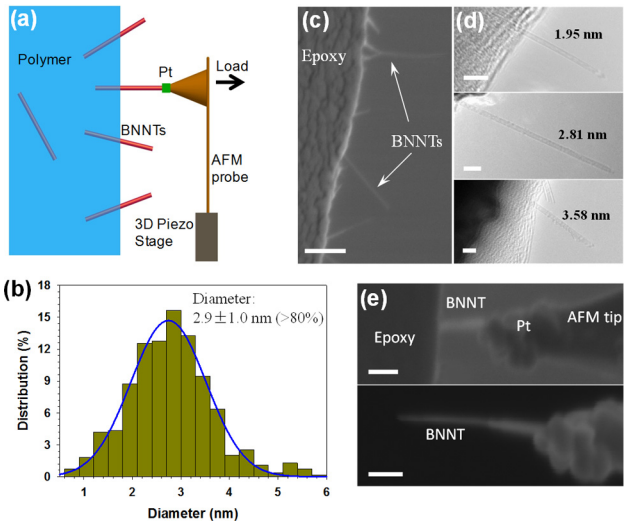

FIG. 1. *In situ* SEM nanomechanical single-tube pull-out measurement. (a) 2D testing schematic and (b) diameter distribution of the dispersed BNNTs measured by AFM ($n = 550$). (c) A BNNT-epoxy thin-film composite sample with protruding BNNTs (*scale bar* 500 nm), (d) HRTEM images of three protruding BNNTs (*scale bars* 10 nm), and (e) selected snapshots of one representative single-tube pull-out measurement (*scale bars* 200 nm).

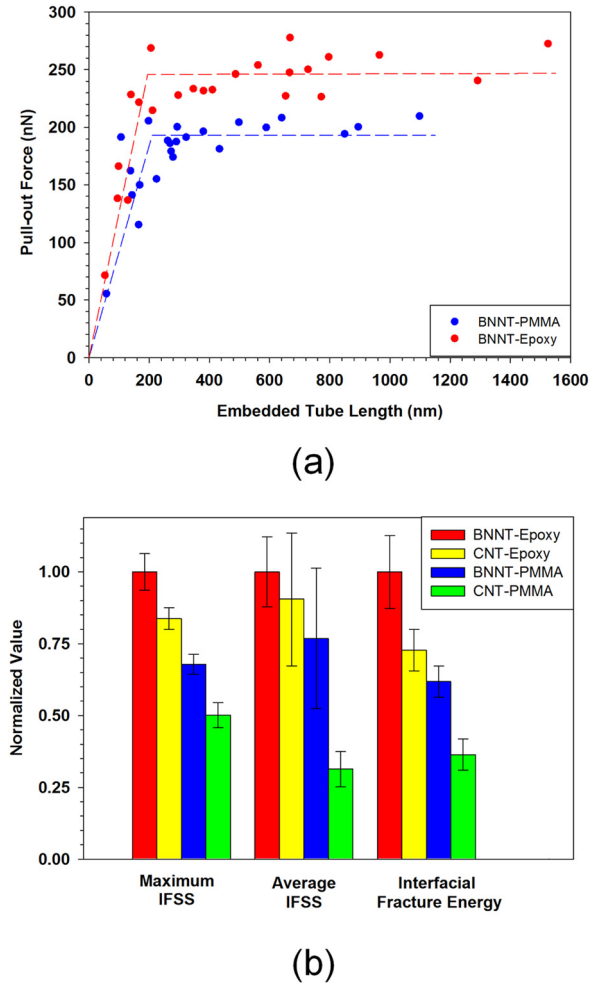

FIG. 2. (a) The measured dependences of the pull-out load on the embedded length for both BNNT-PMMA and BNNT-epoxy interfaces. The dashed lines represent the respective linear fitting curves to the data sets whose embedded tube lengths are below or above the critical embedded length. (b) Comparison of the diameter-weighted IFSS and IFE for four types of nanotube-polymer interfaces. The values on CNT-PMMA and CNT-epoxy interfaces are calculated based on the data reported in Refs. 17 and 18, respectively. All quantities are normalized with respect to the values of BNNT-epoxy interfaces.

polymer matrices employed in this study. The tested BNNT-polymer interfaces were prepared inside sandwiched polymer/tube/polymer thin-film composites by following a previously reported protocol.[17,18] In brief, the polymer was first dissolved in organic solvent, and then spin-coated on a clean silicon wafer to form the first polymer layer. Subsequently, a dispersed BNNT solution was deposited on top of the polymer layer, followed by a deposition of another polymer layer on top. After curing or drying, the BNNT-embedded thin-film composite was broken to expose the embedded tubes as straight free-standing cantilever structures, as exemplified by the SEM image shown in Figure 1(c) as well as the high resolution transmission electron microscopy (HRTEM) image shown in Figure 1(d). HRTEM measurements confirm that those protruding structures are individual tubes, whose diameters are consistent with the values obtained from AFM measurements.

The nanomechanical single-tube pull-out tests were conducted on a number of BNNT-PMMA and BNNT-epoxy samples that were prepared using the same batch of dispersed BNNTs. A representative single-tube pull-out measurement is exhibited in Figure 1(e). An AFM tip was first controlled to approach and subsequently welded, by means of electron beam induced deposition (EBID) of Pt,[23] to the free end of a protruding BNNT from a BNNT-epoxy composite sample. Subsequently, the grabbed tube was fully pulled out of the polymer. The applied pull-out load (P) and the embedded tube length (l) are measured to be 253 nN and 563 nm, respectively. It is noticed that the surface of the originally protruding segment of the tube was also covered by Pt by diffusion during the Pt deposition. The resulting noticeable increase of the diameter of the protruding structure facilitates the measurement of the actual embedded tube length.

Figure 2(a) shows the respective dependences of the pull-out load on the embedded length for both BNNT-PMMA ($n = 23$) and BNNT-epoxy ($n = 23$) interfaces, both of which exhibit a similar trend. The pull-out load first increases with the embedded length and reaches a plateau, and then remains constant with a fairly narrow force fluctuation range even with a several-fold increase of the embedded length. The observed P versus l relationship is a clear sign of the shear lag effect on the BNNT-polymer interfaces.[17,18,24] The shear lag effect describes the failure mechanism of the tube-polymer interface by considering the nanotube pull-out as an interfacial debonding process through crack initiation and propagation. When the embedded length exceeds a threshold value named as "critical embedded length," the interfacial debonding leads to a plateau in the measured P versus l curve. By fitting the experimental data set using a two-segment linear-fitting curve, the critical embedded length l_c, which is defined at the junction of the two linear fitting lines, is measured to be about 210 nm for BNNT-PMMA interfaces and about 195 nm for BNNT-epoxy interfaces. The pull-out load for $l > l_c$ is found to be 193 ± 10 nN (for BNNT-PMMA, $n = 15$) and 246 ± 16 nN (for BNNT-epoxy, $n = 15$). Assuming that the tested tubes on both types

TABLE I. The calculated interfacial fracture energy and shear strengths of the BNNT-PMMA and BNNT-epoxy interface based on the *in-situ* nanomechanical single-tube pull-out measurements.

Polymer matrix	BNNT outer diameter (nm)	Interfacial fracture energy (J/m^2)	Interfacial shear strength (MPa)	
			τ_{max}	τ_{ave}
PMMA	1.9	1.03 ± 0.11	493 ± 26	169 ± 54
	2.9	0.29 ± 0.03	219 ± 11	111 ± 35
	3.9	0.12 ± 0.01	125 ± 6	82 ± 26
Epoxy	1.9	1.67 ± 0.22	728 ± 48	222 ± 30
	2.9	0.47 ± 0.06	323 ± 21	145 ± 20
	3.9	0.19 ± 0.03	183 ± 12	108 ± 15

of interfaces have the identical diameter distribution, the pull-out load of BNNT-epoxy interfaces is 27.5% higher than that of BNNT-PMMA interfaces on an average basis, indicating that BNNTs can form stronger binding interfaces with epoxy than PMMA.

We calculate the interfacial shear strength (IFSS) and interfacial fracture energy (IFE) of BNNT-polymer interfaces to better understand their mechanical strengths, in particular, through comparison with data reported on other types of tube/fiber-polymer interfaces. Two types of IFSS quantities are calculated here, including the average IFSS and the maximum IFSS. The average IFSS is calculated based on the whole bonded interfacial area, and is given as $\tau_{ave} = \frac{P}{\pi \times l \times D_{nt}}$, in which D_{nt} is the nanotube outer diameter. Due to the shear lag effect, the average IFSS is only meaningful for $l < l_c$, for which P increases nearly linearly with l. Based on the data shown in Figure 2(a), $\tau_{ave} = 111 \pm 35$ MPa (for BNNT-PMMA) and 145 ± 20 MPa (for BNNT-epoxy), both of which are calculated using the measured median tube diameter, i.e., $D_{nt} = 2.9$ nm. It is noted that the diameters of individual tubes approach the spatial measurement resolution limit of the electron beam, and thus could not be measured precisely during the nanomechanical tests. Therefore, the median tube diameter is employed to evaluate the relevant interfacial strength quantities, which are regarded as the most representative values of BNNT-polymer interfaces. The maximum IFSS occurs at the tube entry position, and is given as[25,26]

$$\tau_{\max} = \frac{2P \times s}{\pi \times {D_{nt}}^2 \times \tanh(2s \times l/D_{nt})}, \quad (1)$$

where s is a parameter given by $s = \sqrt{\frac{E_m}{E_{nt} \times (1+\nu_m) \times \log(t/D_{nt})}}$, in which E_{nt} is the nanotube's Young's modulus, t is the polymer film thickness, and E_m and ν_m are the Young's modulus and Poisson's ratio of polymers, respectively. The IFE of the tube-polymer interface is given as[27]

$$G_c = \frac{2}{\pi^2} \frac{\left(1 + \operatorname{csch}^2(2s \times l/D_{nt})\right)}{E_{nt} \times D_{nt}} \left(\frac{P}{D_{nt}}\right)^2. \quad (2)$$

The following parameters are employed in the calculation of IFSS and IFE: $E_{nt} = 1.07$ TPa;[14] $t_{PMMA} = 1.6\,\mu$m and $t_{Epoxy} = 2\,\mu$m; $E_{m\text{-}PMMA} = 2.0$ GPa and $\nu_{m\text{-}PMMA} = 0.32$;[28] $E_{m\text{-}Epoxy} = 2.8$ GPa;[29] and $\nu_{m\text{-}Epoxy} = 0.33$.[30] Based on the median tube diameter, the maximum IFSS for $l > l_c$ is found to be about 219 ± 11 MPa (for BNNT-PMMA) and 323 ± 21 MPa (for BNNT-epoxy). G_c is calculated to be 290 ± 30 mJ/m^2 (for BNNT-PMMA) and 470 ± 60 mJ/m^2 (for BNNT-epoxy). The IFSS and IFE values are also calculated based on the upper and the lower bounds (1.9 nm and 3.9 nm) of the BNNT diameter range, and are listed in Table I. It can be clearly seen that BNNT-epoxy interfaces possess consistently higher interfacial strengths than BNNT-PMMA interfaces. The IFE of BNNT-epoxy interfaces exceeds that of BNNT-PMMA interfaces by about 62%, while it is about 31% for the average IFSS and about 47% for the maximum IFSS.

CNTs and carbon nanofibers (CNFs) are two types of widely used carbon-based reinforcing additives for polymer nanocomposites. Here, we compare the mechanical strengths of BNNT-polymer interfaces with the reported data in the literature on interfaces formed by using CNTs and CNFs. In particular, the comparison focuses on the data reported on CNT-PMMA[17] and CNT-epoxy[18] interfaces that were recently characterized by using the same nanomechanical pull-out technique. The utilization of double-walled CNTs (2–4.2 nm in outer diameter and 3.1 nm in median diameter) with comparable structure and diameters of the BNNTs employed in the present study and of the same protocols in sample preparation and measurements enables a convincing comparison of the mechanical strengths among these four types of tube-polymer interfaces. To account for the difference in the diameter distribution of the employed CNTs and BNNTs, we calculate and compare the diameter-weighted interfacial strength quantities by using $\Gamma^* = \sum[P(D_{nt}) \times \Gamma(D_{nt})] / \sum P(D_{nt})$, where Γ refers to one of the interfacial strength quantities and Γ^* is the corresponding diameter-weighted value; $P(D_{nt})$ is the nanotube diameter distribution probability function within the lower and the upper bounds of the measured tube diameter range. Figure 2(b) shows the comparison of the mechanical strengths among the four types of interfaces formed by BNNT/CNT with PMMA/epoxy based on the diameter-weighted IFSS and IFE on a normalized basis. For all three interfacial strength quantities, the data of BNNT-polymer interfaces are statistically higher than those of the comparable CNT-polymer interfaces. For example, the maximum IFSS of BNNT-PMMA interfaces is found to be 35% higher than that of CNT-PMMA interfaces, while a 19.5% increase is observed on BNNT-epoxy interfaces as compared with CNT-epoxy interfaces. Similar phenomenon is also observed in the comparisons with the reported data in the literature that were obtained using different testing techniques. For example, both the average and the maximum IFSS of the BNNT-epoxy interfaces are substantially higher than those of the comparable interfaces formed with CNFs ($\tau_{ave} = 106$ MPa and $\tau_{max} = 224$ MPa).[31] The average IFSS of BNNT-epoxy interfaces is substantially higher than the data (6–30 MPa) on CNT-epoxy interfaces reported by Wagner *et al.*[24] and Lou *et al.*[32] All these findings consistently show that BNNTs are capable of forming stronger binding interfaces with polymers than CNTs or CNFs, indicating a superior load transfer capacity of BNNT-polymer interfaces.

The strength of nanotube-polymer interfaces is ultimately determined by the interfacial binding interaction between nanotubes and polymer matrices. Due to the

polarized nature of B-N bonds, both van der Waals (vdW) and Coulomb interactions contribute to the BNNT-polymer binding strength. In the MD simulation, we investigate the binding interactions of a double-walled BNNT of 6 nm in length and 3.1 nm in outer diameter with PMMA and epoxy. Instead of using a large volume of polymer matrices that makes simulations prohibitively expensive, our MD study focuses on the interfacial binding interaction between one BNNT and a short model polymer chain. Figure 3(a) shows the employed model PMMA (eight monomer units, 122 atoms in total) and epoxy (two Epon 828 units and one curing agent unit, 114 atoms in total) chains. The MD simulations are carried out by using the OPLS-AA force field[33] and based on the following non-bonded interaction potential: $E_{nonbonded} = \sum_{ij}[q_i q_j / r_{ij} + 4\varepsilon_{ij}((\sigma_{ij}/r_{ij})^{12} - (\sigma_{ij}/r_{ij})^{6})]$, where the first term in the series represents the Coulomb energy, and the second term represents the vdW energy that is calculated based on 12–6 Lennard-Jones (*L-J*) potential. r_{ij} is the distance between two atoms i and j, ε_{ij} is the depth of the potential well, and σ_{ij} is the distance corresponding to zero inter-atom potential. q_i and q_j are the electrical charges on atom i and j, respectively. Lorentz-Berthelot mixing rules are employed to calculate the *L-J* coefficients, which are given as $\sigma_{ij} = (\sigma_{ii} + \sigma_{jj})/2$ and $\varepsilon_{ij} = \sqrt{\varepsilon_{ii}\varepsilon_{jj}}$. The following *L-J* coefficients are employed for *C*, *B*, and *N* atoms: $\sigma_C = 0.337$ nm; $\sigma_B = 0.345$ nm; $\sigma_N = 0.337$ nm; $\varepsilon_C = 2.64$ meV; $\varepsilon_B = 4.16$ meV; and $\varepsilon_N = 6.28$ meV.[34–36] The charges on BNNTs $q_B = 0.37e$ and $q_N = -0.37e$ are employed.[37,38] The partial charges on the model PMMA and epoxy chains are adopted from prior MD studies,[39–42] and are shown in Figure S2.[43]

Figure 3(b) shows the respective trajectories of the interfacial binding energy during the relaxation of the model epoxy and PMMA chains on the BNNT surface. The results show that both polymer chains react spontaneously to the binding interaction with the BNNT surface and reach steady-state binding energy state within 5 ps (for PMMA) and 20 ps (for epoxy). The steady-state binding energy is found to be about −82.6 kcal/mol for epoxy and about −65.1 kcal/mol for PMMA. The vdW interactions contribute to about 85.2% of the total binding energy on the BNNT-epoxy interface, and the remaining 14.8% is contributed by the Coulomb interactions. Similar binding energy contributions are also observed for the BNNT-PMMA interface. On a per-atom basis, the BNNT-epoxy binding energy is found to be 35.8% higher than the BNNT-PMMA binding energy, which is consistent with the experimental observation.

The MD simulations also provide insights into the binding mechanism on BNNT-polymer interfaces that possess higher strength as compared with interfaces formed with CNTs. Figure 3(c) shows the comparison of the respective steady-state interfacial binding energies of the model PMMA and epoxy chains with the same-diameter BNNT and CNT. The data show that the total binding energy on BNNT-epoxy interfaces is 71.7% higher than that of CNT-epoxy interfaces, the latter of which is based purely on vdW interactions. It is noted that 46.4% of the observed increase is attributed to the higher vdW interaction on BNNT-epoxy interfaces, while the remaining 25.3% increase is ascribed to the Coulomb interaction. Similar phenomena are also exhibited in the comparison of BNNT-PMMA and CNT-PMMA

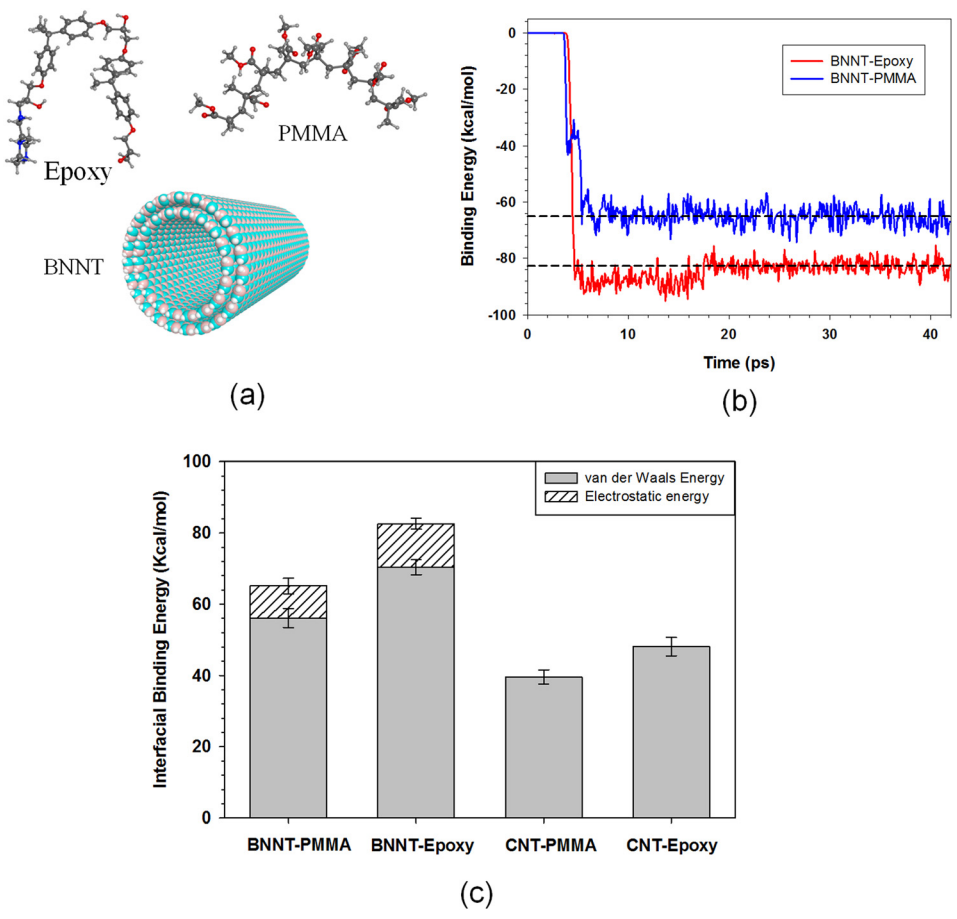

FIG. 3. (a) The molecular structures of the model epoxy and PMMA chains and the BNNT that are employed in the MD simulation. (b) The calculated trajectories of the intermolecular interaction energy between the model epoxy and PMMA chains and the same BNNT during the polymer relaxation process. The dashed lines indicate the average steady-state binding energies. (c) Comparison of interfacial binding energy of the model BNNT and CNT with the model PMMA and epoxy chains.

interfaces. The higher vdW binding interactions observed on BNNT-polymer interfaces can be attributed to the fact that both *B* and *N* atoms possess deeper potential wells as compared with *C* atoms. The MD simulations results support the experimentally observed higher strength of BNNT-polymer interfaces, as compared with CNT-polymer interfaces.

In summary, we report experimental measurements on the strength of BNNT-polymer interfaces using *in situ* nanomechanical single-tube pull-out techniques. Our nanomechanical measurements reveal that BNNTs can form much stronger binding interfaces with polymers than comparable CNTs and that the interfacial strength of BNNT-epoxy interfaces is higher than that of BNNT-PMMA interfaces. The observed superior load transfer capacity of BNNT-polymer interfaces is ascribed to both the polarized nature of B-N bonds and the high bonding potentials of B and N atoms, which are supported by MD simulations. The findings of extraordinary load transfer capacity of BNNT-polymer interfaces suggest that BNNTs are excellent reinforcing nanofiller materials for light-weight and high-strength polymer nanocomposites.

This work was funded by U.S. Air Force Office of Scientific Research—Low Density Materials Program under Grant Nos. FA9550-11-1-0042, FA9550-10-1-0451, and FA9550-15-1-0491. The Raman measurements were performed using a facility that was supported by an NSF MRI Award (No. CMMI-1429176). The simulations were performed at the Georgia Advanced Computing Resource Center at the University of Georgia.

[1]Y. Zhang, K. Song, J. Meng, and M. L. Minus, ACS Appl. Mater. Interfaces **5**, 807 (2013).
[2]X. Tao, L. Dong, X. Wang, W. Zhang, B. J. Nelson, and X. Li, Adv. Mater. **22**, 2055 (2010).
[3]A. Rubio, J. L. Corkill, and M. L. Cohen, Phys. Rev. B **49**, 5081 (1994).
[4]N. G. Chopra, R. J. Luyken, K. Cherrey, V. H. Crespi, M. L. Cohen, S. G. Louie, and A. Zettl, Science **269**, 966 (1995).
[5]C. Zhi, Y. Bando, T. Terao, C. Tang, H. Kuwahara, and D. Golberg, Adv. Funct. Mater. **19**, 1857 (2009).
[6]X. Wei, M.-S. Wang, Y. Bando, and D. Golberg, Adv. Mater. **22**, 4895 (2010).
[7]N. G. Chopra and A. Zettl, Solid State Commun. **105**, 297 (1998).
[8]R. Arenal, M.-S. Wang, Z. Xu, A. Loiseau, and D. Golberg, Nanotechnology **22**, 265704 (2011).
[9]E. Hernandez, C. Goze, P. Bernier, and A. Rubio, Phys. Rev. Lett. **80**, 4502 (1998).
[10]H. M. Ghassemi, C. H. Lee, Y. K. Yap, and R. S. Yassar, J. Appl. Phys. **108**, 024314 (2010).
[11]D.-M. Tang, C.-L. Ren, X. Wei, M.-S. Wang, C. Liu, Y. Bando, and D. Golberg, ACS Nano **5**, 7362 (2011).
[12]A. P. Suryavanshi, M.-F. Yu, J. Wen, C. Tang, and Y. Bando, Appl. Phys. Lett. **84**, 2527 (2004).
[13]D. Golberg, P. M. F. J. Costa, O. Lourie, M. Mitome, X. Bai, K. Kurashima, C. Zhi, C. Tang, and Y. Bando, Nano Lett. **7**, 2146 (2007).
[14]Y. Zhao, X. Chen, C. Park, C. C. Fay, S. Stupkiewicz, and C. Ke, J. Appl. Phys. **115**, 164305 (2014).
[15]M. Zheng, X. Chen, C. Park, C. C. Fay, N. M. Pugno, and C. Ke, Nanotechnology **24**, 505719 (2013).
[16]M. L. Cohen and A. Zettl, Phys. Today **63**(11), 34 (2010).
[17]X. Chen, M. Zheng, C. Park, and C. Ke, Small **9**, 3345 (2013).
[18]X. Chen, L. Zhang, M. Zheng, C. Park, X. Wang, and C. Ke, Carbon **82**, 214 (2015).
[19]M. W. Smith, K. C. Jordan, C. Park, J.-W. Kim, P. T. Lillehei, R. Crooks, and J. S. Harrison, Nanotechnology **20**, 505604 (2009).
[20]A. L. Tiano, C. Park, J. W. Lee, H. H. Luong, L. J. Gibbons, S.-H. Chu, S. Applin, P. Gnoffo, S. Lowther, H. J. Kim, P. M. Danehy, J. A. Inman, S. B. Jones, J. H. Kang, G. Sauti, S. A. Thibeault, V. Yamakov, K. E. Wise, J. Su, and C. C. Fay, in *Nanosensors Biosensors, and Info-Tech Sensors and Systems 2014* (San Diego, California, USA, 2014), pp. 1–19.
[21]M. Zheng, X. Chen, I.-T. Bae, C. Ke, C. Park, M. W. Smith, and K. Jordan, Small **8**, 116 (2012).
[22]M. Zheng, C. Ke, I.-T. Bae, C. Park, M. W. Smith, and K. Jordan, Nanotechnology **23**, 095703 (2012).
[23]C. H. Ke, N. Pugno, B. Peng, and H. D. Espinosa, J. Mech. Phys. Solids **53**, 1314 (2005).
[24]A. H. Barber, S. R. Cohen, A. Eitan, L. S. Schadler, and H. D. Wagner, Adv. Mater. **18**, 83 (2006).
[25]P. S. Chua and M. R. Piggott, Compos. Sci. Technol. **22**, 33 (1985).
[26]H. L. Cox, Br. J. Appl. Phys. **3**, 72 (1952).
[27]K. R. Jiang and L. S. Penn, Compos. Sci. Technol. **45**, 89 (1992).
[28]J. Zeng, B. Saltysiak, W. S. Johnson, D. A. Schiraldi, and S. Kumar, Compos. Part B Eng. **35**, 173 (2004).
[29]*Epon Resin Structural Reference Manual* (Resolution Performance Products LLC, 2001).
[30]C. May, *Epoxy Resins: Chemistry and Technology*, 2nd ed. (Marcel Dekker, 1988).
[31]T. Ozkan, Q. Chen, and I. Chasiotis, Compos. Sci. Technol. **72**, 965 (2012).
[32]Y. Ganesan, C. Peng, Y. Lu, P. E. Loya, P. Moloney, E. Barrera, B. I. Yakobson, J. M. Tour, R. Ballarini, and J. Lou, ACS Appl. Mater. Interfaces **3**, 129 (2011).
[33]W. L. Jorgensen, D. S. Maxwell, and J. Tirado-Rives, J. Am. Chem. Soc. **118**, 11225 (1996).
[34]J. H. Lee, J. Korean Phys. Soc. **49**, 172 (2006).
[35]D. Baowan and J. M. Hill, Micro Nano Lett. **2**, 46 (2007).
[36]M. Neek-Amal and F. M. Peeters, Appl. Phys. Lett. **104**, 041909 (2014).
[37]A. T. Nasrabadi and M. Foroutan, J. Phys. Chem. B **114**, 15429 (2010).
[38]C. Y. Won and N. R. Aluru, J. Phys. Chem. C **112**, 1812 (2008).
[39]W.-K. Kim and L. M. Hayden, J. Chem. Phys. **111**, 5212 (1999).
[40]A. Shokuhfar and B. Arab, J. Mol. Model. **19**, 3719 (2013).
[41]J. Q. Liu, T. Xiao, K. Liao, and P. Wu, Nanotechnology **18**, 165701 (2007).
[42]P. H. Lin and R. Khare, Macromolecules **42**, 4319 (2009).
[43]See supplementary material at http://dx.doi.org/10.1063/1.4936755 for details about the sample characterization and the electrical charge distributions on monomers.